Hydrogen Oxidation and Production Using Nickel-Based Molecular Catalysts with Positioned Proton Relays

ARTICLE *in* JOURNAL OF THE AMERICAN CHEMICAL SOCIETY · FEBRUARY 2006

Impact Factor: 12.11 · DOI: 10.1021/ja056442y · Source: PubMed

6 AUTHORS, INCLUDING:

Aaron D. Wilson
Idaho National Laboratory
21 PUBLICATIONS **850** CITATIONS
SEE PROFILE

James T Muckerman
Brookhaven National Laboratory
237 PUBLICATIONS **6,300** CITATIONS
SEE PROFILE

Article

Hydrogen Oxidation and Production Using Nickel-Based Molecular Catalysts with Positioned Proton Relays

Aaron D. Wilson, Rachel H. Newell, Michael J. McNevin, James T. Muckerman, M. Rakowski DuBois, and Daniel L. DuBois

J. Am. Chem. Soc., **2006**, 128 (1), 358-366• DOI: 10.1021/ja056442y • Publication Date (Web): 09 December 2005

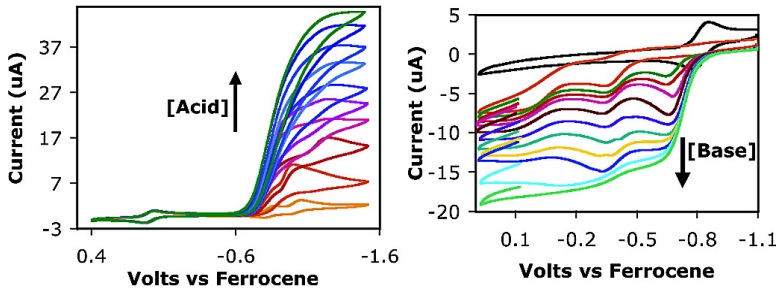

More About This Article

Additional resources and features associated with this article are available within the HTML version:

- Supporting Information
- Links to the 19 articles that cite this article, as of the time of this article download
- Access to high resolution figures
- Links to articles and content related to this article
- Copyright permission to reproduce figures and/or text from this article

View the Full Text HTML

J|A|C|S
ARTICLES
Published on Web 12/09/2005

Hydrogen Oxidation and Production Using Nickel-Based Molecular Catalysts with Positioned Proton Relays

Aaron D. Wilson,[†] Rachel H. Newell,[†] Michael J. McNevin,[†] James T. Muckerman,[§] M. Rakowski DuBois,*[,†] and Daniel L. DuBois*[,‡]

Contribution from the Department of Chemistry and Biochemistry, University of Colorado, Boulder, Colorado 80309, Brookhaven National Lab, P.O. Box 5000, Upton, New York 11973-5000, and National Renewable Energy Laboratory, 1617 Cole Boulevard, Golden, Colorado 80401

Received September 26, 2005; E-mail: mary.rakowski-dubois@colorado.edu; dan_dubois@nrel.gov

Abstract: Highly efficient electrocatalysts for both hydrogen evolution and hydrogen oxidation have been designed, synthesized, and characterized. The catalysts in their resting states are air-stable, mononuclear nickel(II) complexes containing cyclic diphosphine ligands with nitrogen bases incorporated into the ligand backbone. X-ray diffraction studies have established that the cation of $[Ni(P^{Ph}_2N^{Ph}_2)_2(CH_3CN)](BF_4)_2$, **6a**, (where $P^{Ph}_2N^{Ph}_2$ is 1,3,5,7-tetraphenyl-1,5-diaza-3,7-diphosphacyclooctane) is a trigonal bipyramid with bonds to four phosphorus atoms of the two bidentate diphosphine ligands and the nitrogen atom of an acetonitrile molecule. Two of the six-membered rings formed by the diphosphine ligands and Ni have boat conformations with an average Ni- - -N distance to the two pendant bases of 3.4 Å. The cation of $[Ni(P^{Cy}_2N^{Bz}_2)_2](BF_4)_2$, **6b**, (where Cy = cyclohexyl and Bz = benzyl) is a distorted square planar complex. For **6b**, all four six-membered rings formed upon coordination of the diphosphine ligands to the metal are in the boat form. In this case, the average Ni- - -N distance to the pendant base is 3.3 Å. Complex **6a** is an electrocatalyst for hydrogen production in acidic acetonitrile solutions, and compound **6b** is an electrocatalyst for hydrogen oxidation in basic acetonitrile solutions. It is demonstrated that the high catalytic rates observed with these complexes are a result of the positioning of the nitrogen base so that it plays an important role in the formation and cleavage of the H−H bond.

Introduction

Current interest in catalysts for the electrochemical oxidation and production of hydrogen stems from two main sources. One is an increased effort to develop the science and technology required for a hydrogen economy. The use of platinum electrodes in a hydrogen−oxygen fuel cell was described by Mond and Langer in 1889,[1] and Siegl described the use of platinum supported on carbon particles in 1913.[2] Although improvements in catalyst loading have been made, platinum supported on carbon is still the catalyst used in most hydrogen fuel cells today. The development of alternate catalysts that utilize inexpensive materials, such as first-row metal complexes, is an important goal for economic fuel cell design. The recent elucidation of the structures of several hydrogenase enzymes that revealed bimetallic iron complexes and heterobimetallic iron−nickel complexes at the active sites[3−10] provides additional impetus for the development of inexpensive synthetic catalysts for hydrogen oxidation and production.

The active site of the Fe-only hydrogenase enzymes contains a dinuclear iron complex with a bridging 1,3-dithiolate ligand. Although the nature of the dithiolate backbone has not been definitively established by crystallography, structure **1** illustrates one proposed structure in which an azadithiolate promotes the binding and heterolytic cleavage of hydrogen.[3,10] The crystallographic information and structural proposals have been used to develop elegant structural mimics that have provided useful insights into the functioning of hydrogenase enzymes.[11−21] An

[†] University of Colorado.
[§] Brookhaven National Lab.
[‡] National Renewable Energy Laboratory.

(1) Mond, L.; Langer, C. *Proc. R. Soc.* **1889**, *46*, 296.
(2) Siegl, K. Elektrotech. Z. **1913**, *34*, 1317.
(3) Nicolet, Y.; de Lacey, A. L.; Vernède, X.; Fernandez, V. M.; Hatchikian, E. C.; Fontecilla-Camps, J. C. *J. Am. Chem. Soc.* **2001**, *123*, 1596−1601.
(4) Peters, J. W.; Lanzilotta, W. N.; Lemon, B. J.; Seefeldt, L. C. *Science* **1998**, *282*, 1853−1858.
(5) Pereira, A. S.; Tavares, P.; Moura, I.; Moura, J. J. G.; Huynh, B. H. *J. Am. Chem. Soc.* **2001**, *123*, 2771−2782.
(6) Peters, J. W. *Curr. Opin. Struct. Biol.* **1999**, *9*, 670−676.
(7) Volbeda, A.; Garcin, E.; Piras, C.; de Lacey, A. L.; Fernandez, V. M.; Hatchikian, E. C.; Frey, M.; Fontecilla-Camps, J. C. *J. Am. Chem. Soc.* **1996**, *118*, 12989−12996.
(8) Higuchi, Y.; Ogata, H.; Miki, K.; Yasuoka, N.; Yagi, T. *Structure* **1999**, *7*, 549−556.
(9) Garcin, E.; Vernede, X.; Hatchikian, E. C.; Volbeda, A.; Frey, M.; Fontecilla-Camps, J. C. *Structure* **1999**, *7*, 557−565.
(10) Volbeda, A.; Fontecilla-Camps. J. C. *J. Chem. Soc., Dalton Trans.* **2003**, 4030−4038.
(11) Mejia-Rodriguez, R.; Chong, D.; Reibenspies, J. H.; Soriaga, M. P.; Darensbourg, M. Y. *J. Am. Chem. Soc.* **2004**, *126*, 12004−12014.
(12) Justice, A. K.; Linck, R. C.; Rauchfuss, T. B.; Wilson, S. R. *J. Am. Chem. Soc.* **2004**, *126*, 13214−13215.
(13) Lyon, E. J.; Georgakaki, I. P.; Reibenspies, J. H.; Darensbourg, M. Y. *J. Am. Chem. Soc.* **2001**, *123*, 3268−3278.
(14) Zhao, X.; Georgakaki, I. P.; Miller, M. L.; Yarbrough, J. C.; Darensbourg, M. Y. *J. Am. Chem. Soc.* **2001**, *123*, 9710−9711.
(15) Gloaguen, F.; Lawrence, J. D.; Rauchfuss, T. B. *J. Am. Chem. Soc.* **2001**, *123*, 9476−9477.
(16) Lawrence, J. D.; Li, H.; Rauchfuss, T. B.; Bénard, M.; Rohmer, M.-M. *Angew. Chem., Int. Ed.* **2001**, *40*, 1768−1771.

10.1021/ja056442y CCC: $33.50

important fundamental question for the enzymes that remains to be answered is the precise role that the proposed pendant base would play in hydrogen oxidation and production. We report here the design of mononuclear organometallic nickel catalysts that allow us to systematically probe the catalytic chemistry of hydrogen oxidation and proton reduction as the nature and position of the base are varied.

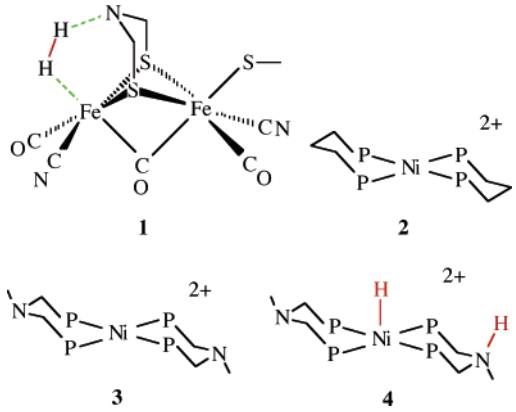

In previous work we investigated the catalytic and thermodynamic properties of relatively simple $[Ni(diphosphine)_2]^{2+}$ complexes in acetonitrile.[22−25] It was found that $[Ni(depp)_2]^{2+}$, **2** (where depp is 1,3-bis(diethylphosphino)propane), which has no pendant base, will slowly oxidize hydrogen with an overpotential of approximately 0.8 V in the presence of an external amine base in solution. Introduction of a nitrogen base into the backbone of the diphosphine ligand as shown for $[Ni(PNP)_2]^{2+}$, **3** (where PNP is bis(diethylphosphinomethyl)methylamine), results in a complex that readily adds hydrogen to form **4**, and **3** is an improved catalyst (a turnover rate of between 0.01 and 0.5 s^{-1} under 1 atm of hydrogen gas) for the electrochemical oxidation of hydrogen at low overpotentials (less than 0.15 V). The enhanced reactivity of **3** compared to that of **2** is attributed to facile inter- and intramolecular proton/hydride exchange. Similar intramolecular proton/hydride exchange reactions have been studied for other transition metal complexes[26−30] but not in the context of catalytic hydrogen oxidation.

To increase the catalytic rate still further we sought to optimize the position of the nitrogen base in the complex. An X-ray diffraction study of **3** indicated that the six-membered rings formed by the chelating PNP ligands are in the more stable chair conformation.[22] For the pendant base and the nickel atom to interact simultaneously with a dihydrogen molecule, the diphosphine ligand must adopt a boat conformation similar to the proposed azadithiolate ligand shown in structure **1** for the active site of hydrogenase. In **1** the boat conformation is enforced by steric interactions with the ligands in the coordination sphere of the second Fe atom. In our studies of the mononuclear nickel complexes, an alternate means for enforcing a boat conformation of a six-membered chelate ring of the ligand is required and has been achieved by employing a cyclic diphosphine ligand. The comparison of the catalytic activities of these new compounds for hydrogen oxidation with those of **2** and **3** provides detailed insights into the role of proton relays in enzymatic and catalytic reactions. By variation of ligand substituents in this system, the thermodynamic properties of the complexes have been modified to also produce very active proton reduction catalysts. Our results confirm that a precisely positioned base results not only in fast proton transport between the solution and the active metal site but also in a significant decrease in the activation barrier for hydrogen−hydrogen bond cleavage or formation.

Results

Synthesis and Characterization of Nickel Complexes with Positioned Pendant Bases. The synthesis of the cyclic ligand **5a** ($P^{Ph}_2N^{Ph}_2$, 1,3,5,7-tetraphenyl-1,5-diaza-3,7-diphosphacyclooctane) from formaldehyde, phenylphosphine, and aniline, as shown in step 1 of reaction 1, was carried out using literature methods.[31a] Reaction of **5a** with $[Ni(CH_3CN)_6](BF_4)_2$ in acetonitrile results in a 90% yield of the red complex $[Ni(P^{Ph}_2N^{Ph}_2)_2(CH_3CN)](BF_4)_2$, **6a**, step 2 of reaction 1. The nitrate salt has been reported previously.[31b] The reaction of formaldehyde, cyclohexylphosphine, and benzylamine produced a mixture of the desired cyclic ligand $P^{Cy}_2N^{Bz}_2$, **5b**, and polymeric material, and further reaction of this mixture with $[Ni(CH_3CN)_6](BF_4)_2$ yielded the purple complex $[Ni(P^{Cy}_2N^{Bz}_2)_2](BF_4)_2$, **6b** in 34% yield. Both products are air-stable in the solid state and in solution, stable to water but insoluble in this solvent, and soluble in polar organic solvents. These complexes have been characterized by ^1H and ^{31}P NMR spectroscopy, elemental analysis, UV−vis spectroscopy, and mass spectroscopy, as detailed in the Experimental Section. All data are consistent with their formulation.

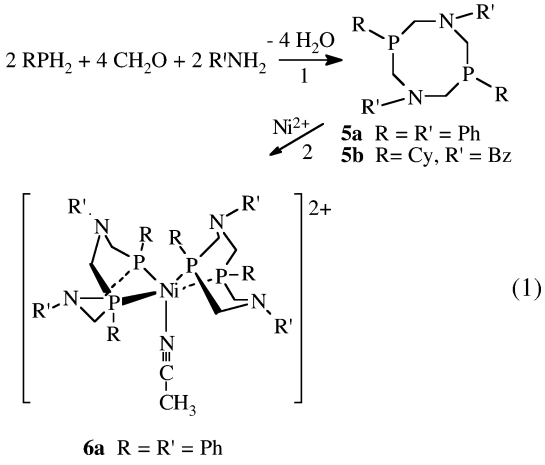

(1)

(17) Evans, D. J.; Pickett, C. *J. Chem. Soc. Rev.* **2003**, *32*, 268−275.
(18) Ott, S.; Kritikos, M.; Åkermark, B.; Sun, L.; Lomoth, R. *Angew. Chem., Int. Ed.* **2004**, *43*, 1006−1009.
(19) Das, P.; Capon, J.-F.; Gloaguen, F.; Pétillon, F. Y.; Schollhammer, P.; Talarmin, J.; Muir, K. W. *Inorg. Chem.* **2004**, *43*, 8203−8205.
(20) Borg, S. J.; Behrsing, T.; Best, S. P.; Razavet, M.; Liu, X.; Pickett, C. J. *J. Am. Chem. Soc.* **2004**, *126*, 16988−16999.
(21) Tard, C.; Liu, X.; Ibrahim, S. K.; Bruschi, M.; De Gioia, L.; Davies, S. C.; Yang, X.; Wang, L.-S.; Sawers, G.; Pickett, C. J. *Nature* **2005**, *433*, 610−613.
(22) Curtis, C. J.; Miedaner, A.; Ciancanelli, R. F.; Ellis, W. W.; Noll, B. C.; DuBois, M. R.; DuBois, D. L. *Inorg. Chem.* **2003**, *42*, 216−227.
(23) Berning, D. E.; Noll, B. C.; DuBois, D. L. *J. Am. Chem. Soc.* **1999**, *121*, 11432−11447.
(24) Berning, D. E.; Miedaner, A.; Curtis, C. J.; Noll, B. C.; DuBois, M. R.; DuBois, D. L. *Organometallics* **2001**, *20*, 1832−1839.
(25) Curtis, C. J.; Miedaner, A.; Ellis, W. W.; DuBois, D. L. *J. Am. Chem. Soc.* **2002**, *124*, 1918−1925.
(26) Lee, D.-H.; Patel, B. P.; Clot, E.; Eisenstein, O.; Crabtree, R. H. *Chem. Commun.* **1999**, 297−298.
(27) Chu, H. S.; Lau, C. P.; Wong, K. Y.; Wong, W. T. *Organometallics* **1998**, *17*, 2768−2777.
(28) Lough, A. J.; Park, S.; Ramachandran, R.; Morris, R. H. *J. Am. Chem. Soc.* **1994**, *116*, 8356−8357.
(29) Custelcean, R.; Jackson, J. E. *Chem. Rev.* **2001**, *101*, 1963−1980.
(30) Ayllon, J. A.; Sayers, S. F.; Sabo-Etienne, S.; Donnadieu, B.; Chaudret, B. *Organometallics* **1999**, *18*, 3981−3990.

Table 1. Selected Bond Distances (Å) and Bond Angles (deg)

$[Ni(P^{Ph}_2N^{Ph})_2(CH_3CN)]^{2+}$		$[Ni(P^{Cy}_2N^{Bz}_2)_2]^{2+}$	
Bond Distances			
Ni(1)−P(1)	2.207(2)	Ni(1)−P(1)	2.2048(13)
Ni(1)−P(2)	2.187(2)	Ni(1)−P(2)	2.2055(14)
Ni(1)−P(3)	2.200(2)		
Ni(1)−P(4)	2.207(2)		
Ni(1)−N(1)	2.046(6)		
Ni(1)- - -N(3)	3.41(2)	Ni(1)- - -N(1)	3.28(7)
Ni(1)- - -N(4)	3.40(4)	Ni(1)- - -N(2)	3.28(8)
N(1)−C(1)	1.11(8)		
Bond Angles			
P(1)−Ni(1)-P(2)	81.53(7)	P(1)−Ni(1)-P(2)	82.74(6)
P(3)−Ni(1)-P(4)	82.63(7)	P(1)−Ni(1)-P(1A)	101.40(7)
P(1)−Ni(1)-P(3)	136.29(7)	P(1)−Ni(1)-P(2A)	157.15(3)
P(2)−Ni(1)-P(4)	177.86(8)	P(2)−Ni(1)-P(2A)	102.23(7)
N(1)−Ni(1)-P(1)	109.27(17)		
N(1)−Ni(1)-P(2)	88.63(16)		
N(1)−Ni(1)-P(3)	114.37(17)		
N(1)−Ni(1)-P(4)	89.61(16)		
Ni(1)−N(1)-C(1)	166.5(6)		

X-ray diffraction studies of these two complexes have been carried out on crystals grown from mixtures of acetonitrile and diethyl ether. For compound **6a**, the crystals consist of $[Ni(P^{Ph}_2N^{Ph}_2)_2(CH_3CN)]^{2+}$ cations and BF_4^- anions. Selected bond distances and angles are given in Table 1, and a drawing of the cation showing only the ipso carbons of the phenyl substituents is shown in Figure 1a. The nickel atom is five-coordinate with bonds to four phosphorus atoms of two bidentate diphosphine ligands and an acetonitrile molecule. The gross structure is that of a trigonal bipyramid with two apical phosphorus atoms and two phosphorus atoms and an acetonitrile molecule in the equatorial positions. From Figure 1a, it can be seen that each $P^{Ph}_2N^{Ph}_2$ ligand forms two six-membered rings upon coordination to the metal, and that one of these is in a chair form and the other is in a boat form. The two nitrogen atoms in the rings with boat conformations are folded toward the nickel atom, and are in a position to interact with either a hydride or dihydrogen ligand.

Compound **6b** crystallizes in the centrosymmetric space group *C*2/*c*. The crystals consist of $[Ni(P^{Cy}_2N^{Bz}_2)_2]^{2+}$ cations, BF_4^- anions, and two uncoordinated acetonitrile molecules. Selected bond distances and angles are given in Table 1, and Figure 1b is a drawing of the cation showing only the carbons of the cyclohexyl and benzyl substituents directly bound to phosphorus or nitrogen. The nickel atom is four-coordinate with bonds to four phosphorus atoms of two bidentate diphosphine ligands. The structure is intermediate between a square planar and a tetrahedral geometry. The dihedral angle between the two planes defined by the two phosphorus atoms of each diphosphine ligand and nickel is 34.88°, and this tetrahedral distortion from a planar geometry is likely the result of steric interactions between the cyclohexyl substituents. From Figure 1b, it can be seen that all four six-membered rings formed upon coordination of the diphosphine ligands to the metal are in the boat form, and the average Ni−N distance is 3.3 Å. Both five- and four-coordinate geometries similar to those identified here have been observed previously for $[Ni(diphosphine)_2]^{2+}$ complexes.[23,24,32]

An interesting structural feature of these cations is the small P−Ni−P bond angles of the diphosphine ligands, which range from 81.5° to 82.7°. These angles are 6−8° smaller than those observed for the analogous complexes, $[Ni(PNP)_2]^{2+}$ and $[Ni(dmpp)_2(CH_3CN)]^{2+}$ which have P−Ni−P bond angles of 89.7° and 89.1°, respectively (where dmpp is 1,3-bis(dimethylphosphino)propane).[22,23] They are even smaller than the 85.1° P−Ni−P angle observed for $[Ni(dmpe)_2(CH_3CN)]^{2+}$ (where dmpe is 1,2-bis(dimethylphosphino)ethane), which forms five-membered chelate rings on coordination to nickel.[23] Presumably the small P−Ni−P bond angles observed for **6a** and **6b** are caused by the constraint of the second six-membered ring in the cyclic ligands.

Reactions of 6a and 6b with H_2. The tetrafluoroborate salt of **6a** in acetonitrile reacts rapidly and reversibly with one atmosphere of dihydrogen in the presence of the external base anisidine to form $[HNi(P^{Ph}_2N^{Ph}_2)_2]^+$, **7a**, and protonated base,

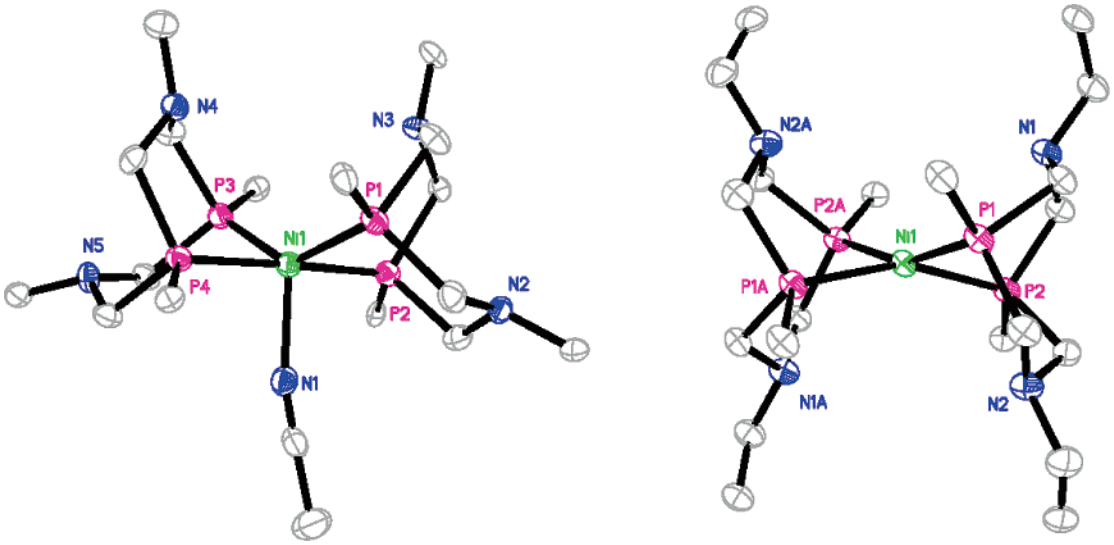

(a) **(b)**

Figure 1. (a) Drawings of the $[Ni(P^{Ph}_2N^{Ph}_2)_2(CH_3CN)]^{2+}$ cation, **6a**, and (b) the $[Ni(P^{Cy}_2N^{Bz}_2)_2]^{2+}$ cation, **6b**, showing the atom numbering schemes. Thermal ellipsoids are shown at 50%.

as shown in reaction 2. The presence of a hydride ligand in complex **7a** is confirmed by the observation of a pentet at −8.1 ppm. The chemical shift and the observed coupling ($^2J_{PH}$ = 30.5 Hz) of this proton to four equivalent phosphorus atoms are diagnostic of this class of compounds. The reversibility of this reaction is confirmed by an increase in the ratio of **7a**/**6a** when the hydrogen pressure is increased and the reformation of the original distribution of products when the pressure is released to one atmosphere. Purging the solution with nitrogen gas results in the reformation of only **6a**. Integration of the ^{31}P and ^{1}H NMR spectra of reaction 2 was used to establish the ratios of **7**/**6** and anisidine/anisidinium. These ratios and the activity of H_2 gas can be used to calculate an equilibrium constant of 0.30 ± 0.06 atm^{-1} for reaction 2 (K = [**7a**] × [HBase$^+$]/P_{H2} × [**6a**] × [Base]). Reaction 2 can also be used as part of a thermodynamic cycle to determine a hydride acceptor ability of −60 kcal/mol for **6a** (see Supporting Information). This hydride acceptor ability is more positive than that observed for the closely related complex $[Ni(PNP)_2]^{2+}$, **3**, which has a hydride acceptor ability of −67 kcal/mol.[22] This is attributed to the smaller P−N−P bond angles of **6** compared to those of **3**, because the hydride acceptor ability increases (becomes more negative) with increasing chelate bite size.[33]

$$\underset{\textbf{6a}}{[Ni(P^{Ph}{}_2N^{Ph}{}_2)_2(CH_3CN)]^{2+}} + H_2 + \text{Base} \leftrightarrow \underset{\textbf{7a}}{[HNi(P^{Ph}{}_2N^{Ph}{}_2)_2]^+} + \text{HBase}^+ \qquad \text{Base} = \text{anisidine} \qquad (2)$$

Complex **6b** reacts with hydrogen in the absence of an external base, but the structures of the hydrogen addition product, **7b**, have not been established in detail. One possible structure is shown in eq 3. The ^{1}H and ^{31}P NMR spectra of **7b** at room temperature are broad, and a nickel hydride resonance is not observed. At −80 °C the ^{31}P NMR spectrum shows two AB quartets and two singlets, consistent with the formation of four different isomers that arise from different ligand conformations. More detailed studies to determine the structures of the isomers are in progress and will be reported in a subsequent paper.

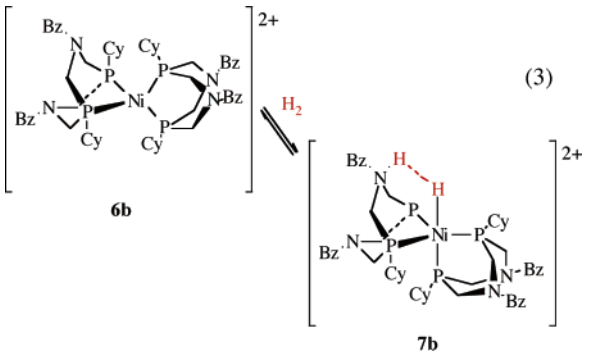

(3)

The formation of the hydrogen adduct is a reversible process when solutions of **7b** are purged with nitrogen gas, as verified by NMR and UV−vis spectroscopy as well as cyclic voltammetry. The reaction of **6b** as a function of hydrogen pressure has been monitored by visible spectroscopy as shown in Figure 2. From these data, an equilibrium constant of 190 ± 20 atm^{-1} was calculated using 1 atm of hydrogen as the standard state. This equilibrium constant can be used to calculate a free energy of −3.1 kcal/mol for hydrogen addition to **6b** at 21.5 ± 2 °C.

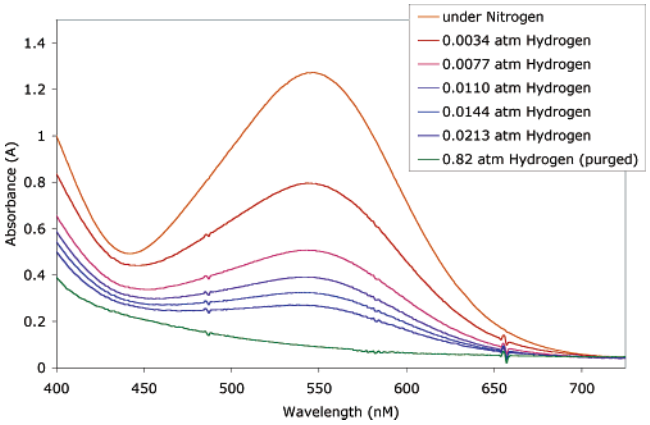

Figure 2. Titration of **6b** with hydrogen in acetonitrile solution at 21°C. Each spectrum was recorded after stirring the solution for 1 h to permit equilibration.

Although **7b** exists in several conformations at room temperature, leading to broad NMR spectra, deprotonation of the ligand in **7b** by triethylamine cleanly forms the monohydride $[HNi(P^{Cy}{}_2N^{Bz}{}_2)_2]^+$, **8b** (reaction 4). The ^{1}H NMR spectrum of **8b** exhibits a pentet assigned to the hydride resonance at −10.7 ppm ($^2J_{PH}$ = 19.4 Hz) and a corresponding singlet in the proton-decoupled ^{31}P NMR spectrum (14.1 ppm), consistent with other hydrides of this type.[22−25] Oxidation of **8b** in the presence of hydrogen and a base leads to catalytic hydrogen oxidation as discussed below.

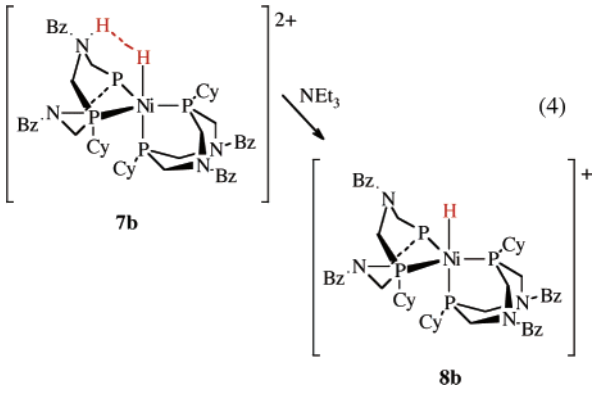

(4)

Electrochemical Studies. A cyclic voltammogram of **6a** in acetonitrile consists of a reversible (ΔE_p = 77 mV at a scan rate of 0.100 V/s), one-electron reduction wave at −0.84 V vs the ferrocene/ferrocenium couple, and a second variable reduction wave at −1.02 V (Figure 3, bottom orange scan). In benzonitrile solutions, the second reduction wave exhibits the characteristic shape of a one-electron, diffusion-controlled wave. Controlled potential electrolysis of an acetonitrile solution of

(31) (a) Märkl, V. G.; Jin, G. Y.; Schoerner, C. *Tetrahedron Lett.* **1980**, *21*, 1409−1412. (b) Khairullina, R. G.; Rusetskii, O. I.; Gorokhovskaya, V. I.; Nikonov, G. N. *Zh. Neorg. Khim.* **1985**, *30*, 2838. (c) For other metal complexes with this ligand type, see: Novikova, E. V.; Karasik, A. A.; Hey-Hawkins, E.; Belov, G. P. *Russ. J. Coord. Chem.* **2005**, *31*, 260−268 and references within.

(32) Miedaner, A.; Haltiwanger, R. C.; DuBois, D. L. *Inorg. Chem.* **1991**, *30*, 417−427.

(33) Raebiger, J. W.; Miedaner, A.; Curtis, C. J.; Miller, S. M.; DuBois, D. L. *J. Am. Chem. Soc.* **2004**, *126*, 5502−5514.

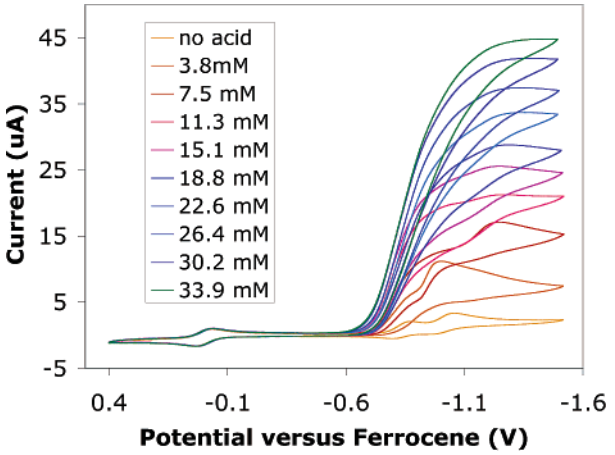

Figure 3. Successive cyclic voltammograms of a 6.4×10^{-4} M solution of **6a** at increasing concentrations of triflic acid as indicated in the legend. Conditions: scan rate = 50 mV/s, acetonitrile solvent, 0.3 M NBu_4BF_4 as supporting electrolyte, glassy carbon working electrode. Potentials are referenced to the ferrocene/ferrocenium couple (wave shown at 0.0 V).

6a at a potential of −0.9 V resulted in the passage of 0.9 faraday of charge per mole of complex, consistent with a one-electron reduction of Ni(II) to Ni(I) at the first reduction wave. The somewhat variable appearance of the second reduction wave in acetonitrile, assigned to the Ni(I)/(0) couple, is attributed to precipitation of the Ni(0) complex on the electrode surface. Plots of i_p vs the square root of the scan rate are linear for these two waves in benzonitrile, indicating that the electron-transfer reactions are diffusion-controlled.

The cyclic voltammogram of **6b** in acetonitrile is similar to that of **6a** with the Ni(II/I) and NiI/0) reductions observed at −0.80 and −1.28 V, respectively. Although the phosphorus and nitrogen substituents in **6b** are more electron donating than those in **6a**, the expected cathodic shifts in the reduction potentials for **6b** are largely counteracted by the lower coordination number for this complex.

Electrocatalytic Studies. (a) Hydrogen Production. Figure 3 shows cyclic voltammograms of **6a** recorded on acetonitrile solutions with different concentrations of triflic acid. It can be seen that in the presence of triflic acid, **6a** exhibits a catalytic wave for the reduction of protons with a half-wave potential (−0.86 V) near the Ni(II/I) couple (−0.84 V). To confirm the production of hydrogen, a controlled potential electrolysis (−0.94 V) was performed on a solution containing 0.88×10^{-3} M catalyst and 0.047 M triflic acid in a sealed flask. After passing 26.8 C of charge, a sample of gas was removed and analyzed by gas chromatography. A current efficiency of 99 ± 5% was calculated for hydrogen production, assuming two electrons are required for each hydrogen molecule.

(b) Hydrogen Oxidation. Figure 4 shows the cyclic voltammograms of **6b** recorded on solutions purged with 0.8 atm of hydrogen and containing different concentrations of triethylamine. The addition of hydrogen (no external base) results in the formation of two new irreversible oxidation waves with peaks at −0.33 and 0.10 V (Figure 4 orange trace) that are assigned to the hydrogen addition product, **7b**. It can be seen that, in the presence of triethylamine, **6b** exhibits a catalytic wave for the oxidation of hydrogen with a half-wave potential of −0.73 V, 0.07 V positive of the Ni(II/I) couple observed in the absence of triethylamine and hydrogen. At triethylamine concentrations above 0.01 M, the current is independent of base

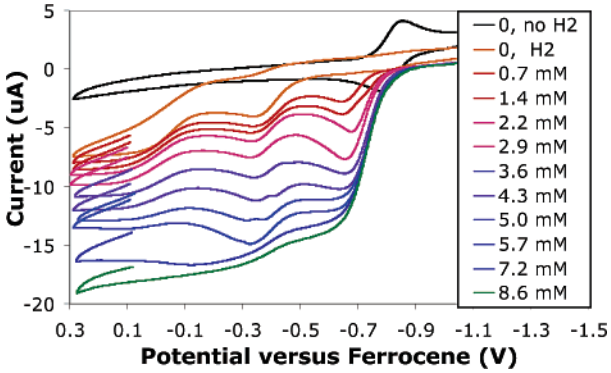

Figure 4. Cyclic voltammogram of a 1.23×10^{-3} M solution of $[Ni(P^{Cy}_2N^{Bz}_2)_2](BF_4)_2$, **6b**, black trace. Remaining cyclic voltammograms were performed on this solution saturated with 0.8 atm of hydrogen gas at increasing concentrations of triethylamine as indicated in the legend. Conditions: scan rate = 100 mV/s, acetonitrile solvent, 0.3 M NBu_4BF_4 as supporting electrolyte, glassy carbon working electrode.

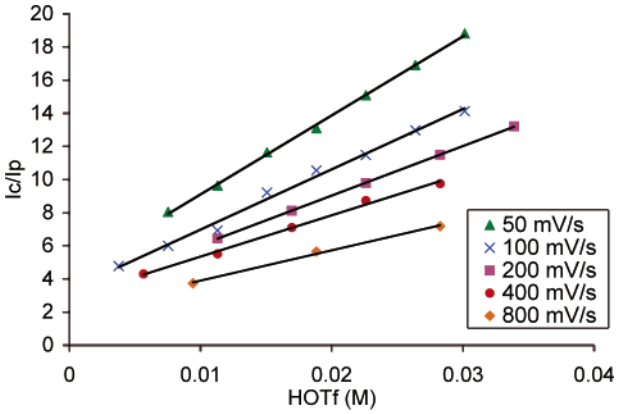

Figure 5. Plots of i_c/i_p versus acid concentration for a 6.4×10^{-4} M solution of $[Ni(P^{Ph}_2N^{Ph}_2)_2](BF_4)_2$, **6a**, in acetonitrile containing 0.3 M NBu_4BF_4 at the indicated scan rates. Lines are best-fit lines to the data.

concentration and depends only on catalyst and hydrogen concentrations (see Kinetic Studies). When the catalytic reaction was carried out in the presence of ca. 5% CO, no measurable effect on the catalytic current was observed.

The data shown in Figures 3 and 4 demonstrate that catalysts for either the production or oxidation of hydrogen can be obtained by varying the substituents on the nitrogen and phosphorus atoms of the $P^R_2N^{R'}_2$ ligand. For **6a**, the protonated nitrogen atom of the ligand is quite acidic. For example, this cation is not protonated by 10 equivalents of cyanoanilinium ion which has a pK_a in acetonitrile of 7.6. As a result, the hydride complex, $[HNi(P^{Ph}_2N^{Ph}_2)(P^{Ph}_2N^{Ph}_2H)]^{2+}$, **7a**, is unstable with respect to hydrogen evolution, and H_2 production is favored for this catalyst (see Supporting Information for more detail on the thermodynamic driving force for H_2 elimination). In contrast, **6b** contains a more basic nitrogen atom, and in this case, equilibrium studies with hydrogen gas, indicate that the formation of $[HNi(P^{Cy}_2N^{Bz}_2)(P^{Cy}_2N^{Bz}_2H)]^{2+}$, **7b**, is favorable by approximately 3 kcal/mol.

Kinetic Studies. Kinetic studies have been carried out for the hydrogen production reaction of **6a**. Figure 5 shows plots of the ratio (i_c/i_p) versus the acid concentration at different scan rates (i_c is the catalytic current, and i_p is the peak current observed for the catalyst in the absence of acid.) Equation 5 shows the relationship between i_c/i_p, the acid concentration for a process that is second order in acid, the number of electrons

involved in the catalytic reaction ($n = 2$ for H_2 production), and the scan rate ν.[34−36]

$$\frac{i_c}{i_p} = \frac{n}{0.4463}\sqrt{\frac{RT}{F}}\sqrt{\frac{k[H^+]^2}{\nu}} = 0.72\sqrt{\frac{k[H^+]^2}{\nu}} \qquad (5)$$

Equation 5 assumes an EC_{cat} mechanism and that the concentration of acid is sufficiently large that its concentration is unaffected during the cyclic voltammetry experiment, i.e., psuedo-first-order conditions. Linear plots are observed for acid concentrations between 0.01 and 0.1 M and for scan rates between 0.05 V/s and 0.8 V/s as shown in Figure 5. The linear plots of (i_c/i_p) versus acid concentration indicate a second-order dependence of the catalytic reaction on acid. A first-order dependence of the catalytic rate on catalyst concentration is also observed (Figure S1). These data are consistent with the following rate law for H_2 production: rate $= k[\text{acid}]^2[\mathbf{6a}]$. From a plot of the slopes shown in Figure 3 vs $1/\nu^{1/2}$ (Figure S2) a third-order rate constant of 1.3×10^4 M^{-2} s^{-1} is obtained. This rate constant is likely a composite of equilibrium and rate constants, and as such it does not provide information on fundamental catalytic steps. However, for a triflic acid concentration of 0.1 M (an acid concentration with which a 0.005 M catalyst solution is compatible), a turnover frequency of 130 mol of H_2 per mole of catalyst per second is observed for this catalyst. This rate is slightly less than that of the Ni−Fe hydrogenases (700 s^{-1}).[14]

Kinetic studies on the hydrogen oxidation reaction promoted by **6b** have established that the reaction rate is independent of base concentration with a 10-fold excess of base and first order in catalyst concentration (Figure S3). Studies with hydrogen pressures ranging from 0.13 to 1.29 atm. indicate a first-order dependence on hydrogen concentration as well (Figure S4). This is consistent with H_2 activation as the rate-limiting step in hydrogen oxidation. Using the i_c/i_p ratio observed under 1 atm of hydrogen and in the presence of excess base, a turnover frequency of 10 mol of hydrogen per mole of catalyst per second (10 s^{-1}) can be calculated for **6b** (see Supporting Information). The catalytic rate of **6b** is much faster than that of **3**, which contains a base in the chair conformation. For **3**, an increase in current is not measurable by cyclic voltammetry under the same conditions, indicating a turnover frequency of less than 0.5 s^{-1}. However, hydrogen addition to **3** to form **4** is more thermodynamically favored ($\Delta G° = -5$ kcal/mol)[22] than the analogous hydrogen addition to **6b** ($\Delta G° = -3$ kcal/mol for reaction 3 as described in the previous section). These results indicate a lower activation barrier for H_2 addition to **6b** compared to **3**. The lower barrier for **6b** is attributed to the easier formation of a transition state that allows simultaneous interaction of H_2 with the nickel atom and the positioned nitrogen base.

Theoretical Calculations. Density functional calculations[37,38] have been performed on the simpler molecule of composition $[(Ni(H_2PCH_2NHCH_2PH_2)_2]^{2+}$ to probe in more detail the interactions within this molecule.[39] Of particular interest is the nature of the transition state involved in the addition of hydrogen to this complex to form the heterolytic cleavage product analogous to **7b**. Structure **9** indicates the geometry of the

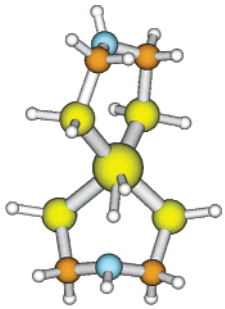

9

transition state (saddle point with a single imaginary vibrational frequency) calculated for this process. Several features are notable. One of the two six-membered rings adopts a boat conformation even though it is not constrained to do so as is true for complexes **6a** and **6b**. Also, the calculated H−H distance of 0.92 Å is consistent with a dihydrogen complex as the transition state, and one of these hydrogen atoms interacts with the pendant nitrogen atom with an N−H distance of 1.56 Å. This interaction results in two very different Ni−H bond distances of 1.56 and 1.84 Å. The transition state therefore consists of an asymmetrically bound dihydrogen ligand that interacts with both the nickel atom and the nitrogen base of the boat form of the diphosphine ligand. Such a transition state is consistent with a positioned pendant base providing a more facile pathway for hydrogen-addition and hydrogen-elimination steps.

Discussion

The results described in this paper demonstrate that turnover frequencies approaching those of Ni−Fe hydrogenase enzymes can be obtained for simple mononuclear nickel complexes. These nickel catalysts can be prepared in two steps from simple, commercially available reagents. They are stable to air in their resting states, and they are readily tuned for hydrogen oxidation or hydrogen production by variation of substituents on the nitrogen and phosphorus atoms of the ligand.

An increased understanding of the role of the proton relay in complexes such as **3**, **6a**, and **6b** has also been obtained. Complex **2**, which lacks a proton relay, can catalyze the oxidation of hydrogen in the presence of an external base, but the reaction is slow, and the overpotentials are large (approximately 0.8 V).[22,25] In addition, the exchange of protons between the bulk solution and the hydride ligand of the corresponding hydride complex is very slow, requiring days for deuterium incorporation from D_2O in CD_3CN. For **3**, which incorporates a proton relay into the backbone of the diphosphine ligand, the rate of proton transfer between the bulk solution and the inner sphere of the nickel complex is dramatically increased. This is accomplished by providing a proton-transfer pathway that does not require significant reorganization of the coordination sphere of the metal complex. Although fast intra-

(34) Delahay, P.; Stiehl, G. L. *J. Am. Chem. Soc.* **1952**, *74*, 3500−3505.
(35) Nicholson, R. S.; Shain, I. *Anal. Chem.* **1964**, *36*, 706.
(36) Saveant, J. M.; Vianello, E. *Electrochim. Acta* **1965**, *10*, 905−920. (e) Saveant, J. M.; Vianello, E. *Electrochim. Acta* **1967**, *12*, 629−646.
(37) Becke, A. D. *J. Chem. Phys.* **1993**, *98*, 5648; Lee, C.; Yang, W.; Parr, R. G. *Phys. Rev. B* **1988**, *37*, 785.
(38) Ditchfield, R.; Hehre, W. J.; Pople, J. A. *J. Chem. Phys.* **1971**, *54*, 724.
(39) Related calculations on the protonation of $[Ni(PNP)_2]^{2+}$ have been reported very recently: Liu, P.; Rodriguez, J. A. *J. Am. Chem. Soc.* **2005**, *127*, 14871−14878.

($k \geq 10^4$ s^{-1}) and intermolecular ($k > 100$ M^{-1} s^{-1} for H_2O in CD_3CN) exchange of the hydride ligand with protons is observed and the overpotential for hydrogen oxidation by **3** is small (less than 0.150 V, a decrease of 0.65 V from **2**), only moderate hydrogen oxidation rates are observed (turnover frequencies between 0.01 and 0.5 s^{-1} under 1 atm of hydrogen).[22]

For complexes **6a** and **6b**, the boat conformations in the ligand force two or more of the pendant bases to adopt a position in close proximity to the nickel atom. A significant increase in the catalyst rate for hydrogen production and hydrogen oxidation is observed compared to **3**, where the chair conformation of the ligand positions the nitrogen atom much further from the metal ion. On the basis of the kinetic and theoretical studies described in this paper, it was found that the positioning of a base in close proximity to the nickel atom results in a decrease in the activation barrier for hydrogen addition and elimination. This decreased barrier is attributed to the simultaneous interaction of nickel and nitrogen with the hydrogen molecule to more easily achieve the transition state.

The results of this work suggest that the following roles for the nitrogen base are important for high catalytic rates not only in this synthetic system, but also in the iron-only hydrogenases: (1) the hydride acceptor and the proton acceptor must be matched in energy so that high energy intermediates are avoided; (2) incorporation of a proton relay is important so that fast proton transfer between the solution and the inner sphere of the metal complex can occur; and (3) precise positioning of the proton relay provides a reduced activation barrier by allowing simultaneous interaction of hydrogen with the proton acceptor and the hydride acceptor within the catalyst.

Experimental Section

General Experimental Procedures. NMR spectra were recorded on a Varian Inova 400 MHz spectrometer. ^1H chemical shifts are reported relative to tetramethylsilane using residual solvent protons as a secondary reference. ^{31}P chemical shifts are reported relative to external phosphoric acid, and all ^{31}P NMR spectra were proton decoupled. All electrochemical measurements were carried out under an N_2 atmosphere in 0.3 M Bu_4NBF_4 in acetonitrile. Cyclic voltammetry experiments were carried out on a Cypress Systems computer-aided electrolysis system. The working electrode was a glassy carbon disk (2 mm diameter), and the counter electrode was a glassy carbon rod. A silver wire was used as a psuedo-reference electrode. Ferrocene was used as an internal standard, and all potentials are referenced to the ferrocene/ferrocenium couple. Gas chromatography was performed using a Perkin-Elmer AutoSystem Gas Chromatograph equipped with a thermal conductivity detector. Chromatograms were obtained and analyzed using Perkin-Elmer Turbochrom Workstation software. The GC was calibrated for H_2 by injecting known quantities of pure gas into the bulk electrolysis cell and then analyzing a 0.1 mL sample of the headspace. A calibration curve was generated from these data.

Kinetics of Catalytic Reactions. Cyclic voltammetry experiments were used to determine the kinetics of the catalytic reactions. In all cases, 1.0 mL of a 0.3 M solution of Bu_4NBF_4 in acetonitrile was used, and ferrocene was added as an internal reference. The working electrode was a glassy carbon disk, the counter electrode was a glassy carbon rod, and an electrode consisting of a silver wire was used as a psuedo-reference electrode.

(a) Proton Reduction. Order with Respect to Acid. This was determined by titration with triflic acid. Catalyst was added to an acetonitrile solution, to make the solution 6.4×10^{-4} M in catalyst. The solution was purged with N_2, and an initial cyclic voltammogram was recorded. Aliquots of triflic acid were added, and the cyclic voltammograms were recorded to determine the catalytic currents. Plots of i_c/i_p versus $[H^+]$ were used to determine the order with respect to H^+ at different scan rates (see Figure 5 of text). The peak current observed for the nickel(II)/(I) couple under one atmosphere N_2 in the absence of acid is i_p, and the peak or plateau current observed in the presence of various amounts of acid is i_c.

Order with Respect to Catalyst. Triflic acid was added to the solution in the cell to make it 0.019 M. Then aliquots of a 6.34 mM stock solution of the catalyst in acetonitrile were added, and cyclic voltammograms were recorded. A plot of the plateau current versus the catalyst concentration was used to determine the order with respect to catalyst (Figure S1).

(b) H_2 Oxidation. Order with Respect to Catalyst. A solution containing 0.014 M NEt_3 was purged with hydrogen. Aliquots of a 7.68 mM stock solution of the catalyst in acetonitrile were added, and cyclic voltammograms were recorded. A plot of the plateau current versus the catalyst concentration was used to determine the order with respect to catalyst Figure S3).

Order with Respect to Hydrogen. A solution that was 0.62 mM in catalyst and 7.2 mM in triethylamine was added to the cell. Aliquots of hydrogen were added to the solution with a gastight syringe over a pressure range of 0.13−1.29 atm, and cyclic voltammograms were recorded. A plot of the plateau current versus the square root of hydrogen pressure was used to determine a first-order dependence on hydrogen (Figure S4).

Order with Respect to [NEt_3]. A solution containing 1.23 mM catalyst was purged with hydrogen. Aliquots of NEt_3 were added, and the cyclic voltammograms were recorded. A plot of the plateau current versus the NEt_3 concentration showed a linear dependence over the first 5−6 equiv of base and no further current increase after ca. 6 equiv.

Effect of Carbon Monoxide on Catalytic Current. An acetonitrile/Bu_4NBF_4 solution (2 mL) that was 1.23 mM in catalyst and 7.2 mM in triethylamine was added to a 4 mL cell, and the solution was purged with hydrogen. CO (0.1 mL at ambient pressure) was injected into the cell, and the solution was stirred prior to each scan. The catalytic current was periodically monitored by cyclic voltammetry for 20 min. A slight decrease in catalytic current was observed over this time period with the final current at 94% of that recorded in the initial scan before CO was added. For comparison, the same experiment was repeated without the addition of CO. A similar slight decrease in catalytic current was observed with the final current at 93% of that recorded initially.

Controlled-Potential Coulometry. A three-necked flask with a stopcock having a total volume of 136 mL was used for bulk electrolysis experiments. One neck was a 24/40 joint that accepted a stainless steel 24/40 fitting with an insulated copper wire running through it. To this was attached a cylinder of reticulated vitreous carbon as a working electrode (1 cm diameter by 2.5 cm length). The other two necks of the flask were 14/20 joints. Both were fitted with glass compartments with Vycor frits on the bottom. One was used as the reference electrode—it was filled with a solution of ferrocene/ferrocenium in acetonitrile, and a tungsten wire was inserted. The other was used as the counter electrode, and it contained a 0.3 M Bu_4NBF_4 acetonitrile solution and a platinum wire. The cell was typically filled with 24 mL of 0.3 M Bu_4NBF_4 in acetonitrile. Triflic acid (0.047 M) and $[Ni(P^{Ph}_2N^{Ph}_2)_2(CH_3CN)](BF_4)_2$ (0.88 mM) were added to the solution. Controlled-potential coulometry was performed at −0.94 V versus the ferrocene/ferrocenium reference electrode. After 26.8 C of charge was applied, samples of the gas in the headspace of the flask were removed via a gastight syringe and analyzed by gas chromatography with the use of a calibration curve to determine the amount of H_2. From these data 6.5 mol H_2 was produced per mole of catalyst, and a current efficiency of 99 ± 5% was calculated for H_2 production.

A similar coulometry experiment carried out on an acetonitrile solution containing $[Ni(P^{Ph}_2N^{Ph}_2)_2(CH_3CN)](BF_4)_2$ (2.96×10^{-5} mmol) in the absence of acid at approximately −0.95 V resulted in the passage

Table 2. Crystal Data for $[Ni(P^{Ph}_2N^{Ph}_2)_2(MeCN)](BF_4)_2$ (**6a**) and $[Ni(P^{Cy}_2N^{Bz}_2)_2](BF_4)_2 \cdot 2(MeCN)$ (**6b**)

	(**6a**)	(**6b**)
formula	$C_{58}H_{59}B_2F_8N_5NiP_4$	$C_{64}H_{94}B_2F_8N_6NiP_4$
formula weight	1182.31	1303.66
temperature	152(2) K	152(2) K
crystal system	orthorhombic	monoclinic
space group	$P2_12_12_1$ (No. 19)	$C2/c$ (No. 15)
unit cell dimensions		
	$a = 12.9803(5)$ $\alpha = 90°$	$a = 17.571(13)$ $\alpha = 90°$
	$b = 18.2873(7)$ $\beta = 90°$	$b = 16.235(11)$ $\beta = 99.754(15)°$
	$c = 23.0460(8)$ $\gamma = 90°$	$c = 23.576(17)$ $\gamma = 90°$
volume	5470.5(4) Å^3	6628.0(8) Å^3
Z	4	4
crystal size, mm^3	$0.25 \times 0.10 \times 0.02$	$0.50 \times 0.36 \times 0.10$
goodness-of-fit on F^2	0.968	0.962
final R indices [$I > 2\sigma(I)$]	R1 = 0.0809, wR2 = 0.1463	R1 = 0.0651, wR2 = 0.1005
R indices (all data)	R1 = 0.1763, wR2 = 0.1753	R1 = 0.1633, wR2 = 0.1888

of 2.65 C of charge. This corresponds to 0.93 faraday per mole of catalyst, and it supports a one-electron process for the first reduction wave. The second reduction wave shows an identical current amplitude as the first and is also assigned as a one-electron process.

Syntheses. All manipulations were performed under an inert atmosphere using standard Schlenk techniques or a glovebox. Solvents were distilled under nitrogen using standard procedures. $[Ni(CH_3CN)_6](BF_4)_2$[40] and 1,3,5,7-tetraphenyl-1,5-diaza-3,7-diphosphacyclooctane ($P^{Ph}_2N^{Ph}_2$)[31] were prepared using literature methods. Cyanoanilinium triflate was prepared by reacting 4-cyanoaniline with triflic acid in ether and washing the resulting solid with ether.

Synthesis of $[Ni(P^{Ph}_2N^{Ph}_2)_2(CH_3CN)](BF_4)_2$ (6a). A mixture of $[Ni(CH_3CN)_6](BF_4)_2$ (0.40 g, 0.80 mmol) and $P^{Ph}_2N^{Ph}_2$ (0.73 g, 1.62 mmol) in acetonitrile (50 mL) was stirred at room temperature for 4 h to form a clear red-orange solution. Reducing the volume to 35 mL and adding diethyl ether (75 mL) resulted in a red powder (0.86 g, 91%). X-ray quality crystals were grown by diffusion of diethyl ether into an acetonitrile solution of the complex at room temperature. Anal. Calcd for $C_{58}H_{59}B_2F_8N_5P_4Ni$: C, 58.92; H, 5.03; N, 5.92. Found: C, 58.63; H, 4.99; N, 5.85. ^{1}H NMR (CD_3CN): δ 7.1 and 7.45 (m, 43 H, Ar-*H*); 4.24 (d, $^2J_{HH} = 14.1$ Hz, 8.0 H, PC*H*$_2$N); 3.93 (d, $^2J_{HH} = 14.1$ Hz, 7.6 H, PC*H*$_2$N); 1.97 (s, 3.1 H, C*H*$_3$CN). ^{31}P NMR (CD_3CN): δ 4.82 (s).

$[Ni(P^{Cy}_2N^{Bz}_2)_2](BF_4)_2$, 6b. In a typical procedure, $CyPH_2$ (4.32 g, 37.5 mmol) and formaldehyde (37% by wt in H_2O, 8.4 mL, 112 mmol) were combined in 20 mL of MeCN and allowed to stir at room temperature for 0.5 h. The solvent was removed under vacuum, and a portion of the resulting oil (1.78 g) was combined with NH_2CH_2Ph (1.08 g, 10.1 mmol) in 40 mL of EtOH and refluxed for 14 h. The solvent was removed by vacuum, leaving a white solid which was washed with three 20-mL portions of 1:3 Et_2O/H_2O and dried overnight under vacuum. Yield: 2.015 g, 4.074 mmol, 81% yield based on amine. ^{31}P NMR in $CDCl_3$ showed a singlet for the major product (85%) at −41 ppm. $[Ni(MeCN)_{6.5}](BF_4)_2$ (0.30 g, 0.60 mmol) and the crude ligand (0.60 g, 1.2 mmol) were combined in 20 mL of MeCN and allowed to stir at room temperature for 4 days. The resulting purple solution, which still contained some white ligand material, was filtered, and the filtrate was reduced to a volume of ~4 mL under vacuum. The addition of ~40 mL of Et_2O resulted in the precipitation of the nickel complex as a purple solid. X-ray quality crystals were obtained by recrystallization of the product from acetonitrile (8 mL)/ Et_2O (30 mL). Yield: 0.28 g, 0.21 mmol, 35% yield, 28% overall. Anal. Calcd for $[Ni(P^{Cy}_2N^{Bz}_2)_2](BF_4)_2 \cdot 2MeCN$, $C_{64}H_{94}B_2F_8N_6P_4Ni$: C, 58.96; H, 7.27; N, 6.45. Found: C, 59.03; H, 7.22; N, 6.46. Mass Spec, *m*/*z*: 1134 and 523 with isotope patterns matching $[Ni(P^{Cy}_2N^{Bz}_2)_2](BF_4)^+$ and $[Ni(P^{Cy}_2N^{Bz}_2)_2]^{+2}$. ^{1}HNMR ($CD_3CN$): δ 7.4 (m, Ar-H, 12.2 protons); 7.2 (m, Ar-H, 7.8 protons); 3.7 (d, 13 Hz, NCH_2Ph, 4.1 protons); 3.5 (d, 13 Hz, NCH_2Ph, 3.9 protons); 3.1 (d, 14 Hz, PCH_2N, 4.0 protons); 2.9 (d, 13 Hz, PCH_2N, 4.0 protons); 2.7 (d, 14 Hz, PCH_2N, 3.9 protons); 2.6 (broad d, 13 Hz, PCH_2N, 4.1 protons); 1.97 (sharp s, Free MeCN, 6.3 protons); 1.95 (broad peak beneath solvent peak, Cy-H, ~4 protons); 1.9 (broad d, 10.8 Hz, Cy-H, 8.0 protons); 1.7 (broad d, 12.0 Hz, Cy-H, 7.9 protons); 1.55 (broad d, 12.4 Hz, Cy-H, 4.2 protons); 1.42 to 1.16 (m, Cy-H, 17.12 protons); 1.0 (broad q, 12.0 Hz, Cy-H, 4.2 protons). ^{31}P NMR (CD_3CN): δ 9.52 (broad s, sharpens when heated).

Equilibration of $[Ni(P^{Ph}_2N^{Ph}_2)_2(CH_3CN)](BF_4)_2$ with H_2 and Anisidine/Anisidinium in Acetonitrile-d_3. In a typical experiment, $[Ni(P^{Ph}_2N^{Ph}_2)_2(CH_3CN)](BF_4)$ (25 mg, 0.021 mmol) and anisidinium triflate ($pK_a = 11.3$)[41] (10 mg, 0.081 mmol) were accurately weighed into an NMR tube and dissolved in acetonitrile-d_3 (0.6 mL). Hydrogen gas was bubbled through the solution for 20 min. The solution was allowed to sit for 10 min and was monitored by ^{1}H NMR and ^{31}P NMR spectroscopy. The reaction came to equilibrium within the time of mixing and was monitored every several hours for 24 h to ensure that the ratios had not changed. The ^{1}H and ^{31}P NMR resonances assigned to $[Ni(P^{Ph}_2N^{Ph}_2)_2(CH_3CN)](BF_4)_2$, **6a**, and $[HNi(P^{Ph}_2N^{Ph}_2)_2](BF_4)$, **8a**, were integrated, and the ratio was used to determine the equilibrium constant for the reaction. The same values were obtained from both the ^{31}P and ^{1}H NMR spectra. Four separate experiments were run to determine the reproducibility. The equilibrium constant ($K = [\mathbf{8a}] \times [HBase^+]/P_{H2} \times [\mathbf{6a}] \times [Base]$) of 0.30 ± 0.06 was used to calculate a hydride donor ability of 59.8 ± 0.4 kcal/mol (see Supporting Information) for $[HNi(P^{Ph}_2N^{Ph}_2)](BF_4)$. Increasing the hydrogen pressure by injecting additional H_2 gas into the NMR tube containing a solution prepared as described above resulted in an increase in the concentration of $[HNi(P^{Ph}_2N^{Ph}_2)_2](BF_4)$, and purging with N_2 gas for 15 min resulted in the observation of only $[Ni(P^{Ph}_2N^{Ph}_2)_2(CH_3CN)](BF_4)_2$. ^{1}H NMR for $[HNi(P^{Ph}_2N^{Ph}_2)_2](BF_4)_2$, **8b**, ($CD_3CN$): δ 6.9 and 7.6 (br m, Ar-*H*); 3.8 (d, $^2J_{HH} = 7.2$ Hz, PC*H*$_2$N); 3.1 (d, $^2J_{HH} = 7.2$ Hz, PC*H*$_2$N); −8.1 (pentet, $^2J_{PH} = 30.5$ Hz, HNi). ^{31}P NMR (CD_3CN): δ 15.65 (s).

Equilibration of $[Ni(P^{Cy}_2N^{Bz}_2)_2](BF_4)_2$ with H_2 in acetonitrile. Aliquots of hydrogen were added via a gastight syringe to a round-bottom flask (487 mL total volume) containing 2 mL of 4.91 mM solution of **6b** in acetonitrile. The flask was fitted with a 2 mm quartz cuvette to permit UV−vis spectral measurements and a sidearm with a gastight septum for introducing gas samples. After addition of each aliquot of H_2 gas, the solution was stirred for 1 h to allow the contents to come to equilibrium. Spectra were recorded after equilibration, and the disappearance of the peak at 545 nm was monitored (see Figure 2). The last data point was taken after the flask had been purged with hydrogen (0.82 atm, ambient pressure in Boulder, CO). An equilibrium constant of 190 ± 20 atm^{-1} was calculated for $K = [\mathbf{7b}]/(P_{H2} \times [\mathbf{6b}])$ using 1 atm of hydrogen as the standard state (see reaction 2 of text).

(40) Hathaway, B. J.; Underhill, A. E. *J. Chem. Soc.* **1960**, 3705−3711.

(41) Edidin, R. T.; Sullivan, J. M.; Norton, J. R. *J. Am. Chem. Soc.* **1987**, *109*, 3945−3953.

This corresponds to a free energy of −3.1 kcal/mol for the binding of H_2 by **6b** in acetonitrile at 21.5 ± 2 °C.

X-ray Diffraction Studies. Crystals of appropriate size were mounted on a glass fiber using Paratone-N oil, transferred to a Siemens SMART diffractometer/CCD area detector, centered in the beam (Mo Kα; $\lambda = 0.71073$ Å; graphite monochromator), and cooled by a nitrogen low-temperature apparatus. Preliminary orientation matrix and cell constants were determined by collection of 60 10-s frames, followed by spot integration and least-squares refinement. A minimum of a hemisphere of data was collected using 0.3° ϖ scans. The raw data were integrated and the unit cell parameters refined using SAINT. Data analysis was performed using XPREP. Absorption correction was applied using SADABS. The data were corrected for Lorentz and polarization effects, but no correction for crystal decay was applied. Structure solutions and refinements were performed (SHELXTL-Plus V5.0) on F^2.

Crystals of **6a** suitable for X-ray diffraction studies were grown from a MeCN/ Et_2O solution at room temperature. Preliminary data indicated a primitive orthorhombic cell. Analysis of all data indicated systematic absences consistent with space group $P2_12_12_1$. The choice of $P2_12_12_1$ (No. 19) was supported by the successful solution and refinement of the structure. All non-H atoms were refined anisotropically. Hydrogens were placed in idealized positions and were included in structure factor calculations but were not refined. It was necessary to restrain B−F bond distances in the anions. The flack parameter refined to 0.0193 with ESD of 0.0220. The conformation was chosen because inversion of the structure gave a value near 1. Crystal data for **6a** and **6b** are shown in Table 2.

Crystals of **6b** suitable for X-ray diffraction studies were grown from a MeCN/ Et_2O solution at room temperature. Preliminary data indicated a primitive monoclinic cell. Systematic absences indicated space group $C2/c$ (No. 15). This was supported by the successful solution and refinement of the structure. All non-H atoms were refined anisotropically. Hydrogens were placed in idealized positions and were included in structure factor calculations but were not refined. Least-squares planes (x,y,z in crystal coordinates) and deviations from them were determined using the *mpla* command in SHELXTL.

Details of the Theoretical Calculations. All calculations on the reaction path of the model catalyst $[Ni(PH_2CH_2NHCH_2PH_2)_2]^{2+}$ were carried out using the UB3LYP hybrid DFT method[37] and the all-electron 6-31G(d,p) basis[38] with the Gaussian 03 program. Coordinates for the calculated structures of $[Ni(PH_2CH_2NHCH_2PH_2)_2]^{2+}$ and the transition state $[(H_2)Ni(PH_2CH_2NHCH_2PH_2)_2]^{2+}$ are given in Tables S12 and S13 of the Supporting Information.

Acknowledgment. This research was supported by the National Science Foundation, Grant Number CHE-0240106. NMR instrumentation used in this work was supported in part by the National Science Foundation CRIF program (CHE-0131003). D.L.D. and J.T.M. acknowledge the support of the United States Department of Energy, Office of Science, Chemical and Biological Sciences Division under contracts No. DE-AC36-99GO10337 and DE-AC02-98CH10886, respectively.

Supporting Information Available: Figures S1−S5; X-ray structural data in CIF format including tables of crystal and refinement data, atomic positional and thermal parameters, and interatomic distances and angles for $[[Ni(P^{Ph}{}_2N^{Ph}{}_2)_2(CH_3CN)](BF_4)_2$ and $[Ni(P^{Cy}{}_2N^{Bz}{}_2)_2](BF_4)_2$. This material is available free of charge via the Internet at http://pubs.acs.org.

JA056442Y